8-1-1999

Anticipating EMI from Coupling Between High-Speed Digital and I/O Lines

Wei Cui

Min Li

Xiao Luo

James L. Drewniak
Missouri University of Science and Technology, drewniak@mst.edu

et. al. For a complete list of authors, see https://scholarsmine.mst.edu/ele_comeng_facwork/1451

Recommended Citation

W. Cui et al., "Anticipating EMI from Coupling Between High-Speed Digital and I/O Lines," *Proceedings of the IEEE International Symposium on Electromagnetic Compatibility (1999, Seattle, WA)*, vol. 1, pp. 189-194, Institute of Electrical and Electronics Engineers (IEEE), Aug 1999.
The definitive version is available at https://doi.org/10.1109/ISEMC.1999.812893

Anticipating EMI From Coupling Between High-Speed Digital and I/O Lines

W. Cui, M. Li, X. Luo*, J. L. Drewniak, T. H. Hubing, T. P. VanDoren, R. E. DuBroff
Electromagnetic Compatibility Laboratory
Department of Electrical and Computer Engineering
University of Missouri-Rolla
Rolla, MO 65409
wcui@ece.umr.edu

*Lucent Technologies Atlanta Works
2000 Northeast Expressway
Norcross, GA 30071

Abstract: The increasing speed of digital circuit design as well as the density of printed circuit board (PCB) layouts often result in more challenging electromagnetic interference (EMI) problems. The coupling between a high-speed digital line and an I/O line can be a primary EMI coupling path, and the attached cable a dominant radiator. This mechanism is studied and modeled herein in a multi-stage modeling fashion. EMI modeling is developed for coupling between the transmission lines, and the attached cable as the EMI antenna. Finally, the EMI is calculated for the coupled noise driving the attached cable. The agreement between the modeled and measured results demonstrates that the modeling method is suitable for estimating the EMI due to high-frequency coupling to I/O lines.

I. Introduction

High-frequency noise at the PCB connector resulting from coupling between high-speed digital and I/O lines can drive the attached cable and result in EMI problems. Quantifying and modeling this EMI mechanism are essential to analyze and evaluate the electromagnetic compatibility (EMC) of a PCB. One useful approach is full-wave modeling of the coupling and the EMI antenna. A hybrid FEM/MOM method has been proposed to resolve the difficulty of numerical electromagnetic modeling of inhomogeneous regions with a fine scale geometry such as a PCB, and an extended cable at a much larger scale [1]. However, the full-wave modeling is usually overwhelmed by the mixed-scale problem. The small geometries of the traces at the PCB level and the large geometries with the EMI antenna consumes dramatic computational resources. An alternative approach is to separate the problem of noise coupling between the transmission lines from the EMI antenna and the radiation problem. This approach is presented herein with the assumptions that the radiation is dominated by the common-mode current on the attached cable, and the radiation from the traces and direct coupling between the traces and the cable are negligible. EMI modeling of the coupling between the transmission lines, effective EMI antenna, and the radiation from the attached cable are developed herein in a multi-stage fashion to address the entire problem.

The coupled transmission-line problem has been studied extensively. In crosstalk analysis, modal decomposition is used to decouple the transmission lines in the frequency domain [2]. The coupled noise is determined by solving the decoupled transmission-line equations. Fast algorithms have been reported to determine the transient response of lossy lines in the time domain [3]. Another common approach in modeling the coupled transmission lines is to use lumped circuit elements. For electrically short transmission lines, a number of cascaded lumped-element sections are used to account for the distributed characteristics [4] [5]. The lumped-element method is also advantageous for fast circuit simulations with SPICE, since other lumped element models can be easily incorporated. IBIS device models, different types of terminations, filtering, and line loss can be handled with this approach. The multiple lumped-element section modeling can yield a good approximation to the exact solutions for the transmission-line equations [5] [6].

Noise at the connector can drive the attached cable against the reference plane of the PCB in a multi-layer PCB design and result in significant EMI. For clock frequencies or harmonics exceeding several hundred megahertz, the ca-

0-7803-5057-X/99/$10.00 © 1999 IEEE

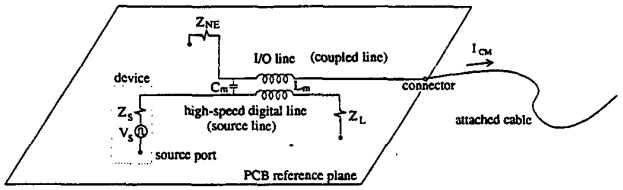

Figure 1. Schematic representation of EMI from a PCB due to coupling to an I/O line.

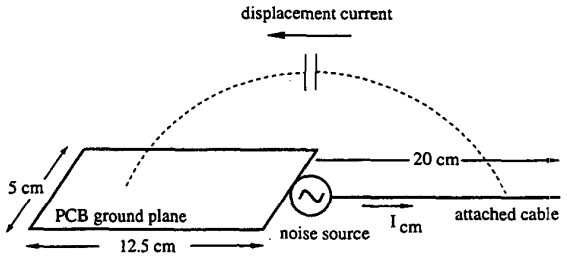

Figure 2. EMI model of the cable attached to a PCB.

ble and the PCB can be of resonant dimensions. The input impedance of a resonant antenna is on the order of 100 Ω, and the cable is easily driven by an effective noise source at the connector. Numerical methods, such as the finite-difference time-domain (FDTD) and finite-element method (FEM), have been employed to determine the input impedance of the attached cable. The EMI antenna modeling is separated from the coupled-line problem, independent of the PCB traces and the dielectric substrate. The radiated fields can be determined from this numerical analysis as well. With the use of the EMI antenna modeling and the calculated radiated fields, the EMI due to coupling to I/O lines can be determined.

II. Multi-stage EMI Modeling of Coupling, EMI Antenna, and Radiation

Coupling from a high-speed digital line to an adjacent I/O line can result in high-frequency noise at the PCB connector. EMI problems arise when the effective noise voltage drives the attached cable. A schematic representation of this mechanism is shown in Figure 1. The EMI modeling for the entire problem is comprised of three distinct aspects: modeling the coupling between the transmission lines, modeling the EMI antenna, and determining the common-mode current on, or related EMI from the attached cable. Appropriate modeling methods are employed to treat these separate problems. The complete analysis is accomplished through a multi-stage modeling approach, which is:

- develop the equivalent circuit models for the coupled transmission lines and determine the per-unit-length parameters;
- determine the input impedance of the EMI antenna;
- use the input impedance of the EMI antenna as a lumped load in the coupled I/O line circuit, and determine the noise voltage driving the EMI antenna using a coupled transmission line model; and,
- determine the common-mode current on the cable or radiated fields for the noise voltage driving the EMI antenna using FDTD modeling.

The coupled transmission lines are modeled first to determine the noise voltage at the connector. The coupled transmission lines are modeled with multiple lumped-element pi-sections [6], and the per-unit-length parameters determined with numerical tools or from measurements. The circuit terminations are derived from the physical circuits or using device models, with the exception of the far-end load of the coupled I/O line, where the cable is attached. At the board connector, the equivalent impedance looking into the attached cable (with the PCB reference as the second terminal) is the input impedance of the EMI antenna, since the noise voltage at the connector drives the cable against the PCB reference plane and extended ground. This EMI antenna, with a structure shown in Figure 2, is modeled with the FDTD method. The input impedance of the EMI antenna is calculated by applying a source voltage at the antenna terminals, i.e., between the cable and PCB reference plane at the connector. To extract the input impedance as a function of frequency, the source voltage used in the FDTD modeling is a sinusoidally modulated Gaussian pulse. The attached cable and the PCB reference plane are modeled as two halves of the EMI antenna. The EMI antenna input impedance is then placed as a lumped load in the coupled transmission-line circuit, and the noise voltage at the connector is determined.

In the FDTD modeling of the EMI antenna, the radiated field ($\vec{E}^{SMGP}$) at 3 m due to the sinusoidally modulated Gaussian pulse source V_s^{SMGP} is also determined. For the noise voltage (V_{noise}^{cl}) determined from the coupled line problem, which drives the EMI antenna, the radiated field $|\vec{E}^{cl}|$ is then calculated from FDTD modeling by

$$|\vec{E}^{cl}| = |\vec{E}^{SMGP}| \times \left| \frac{V_{noise}^{cl}}{V_s^{SMGP}} \right|. \qquad (1)$$

This approach facilitates a single FDTD calculation for a broad frequency range, and circumvents using V_{noise}^{cl} in many sinusoidal source calculations to sweep a frequency range.

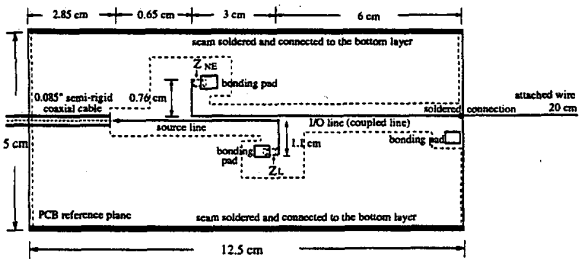

Figure 3. Top view of the test board.

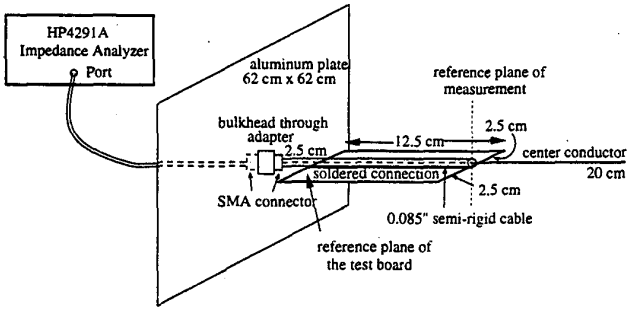

Figure 4. The configuration of the EMI antenna input impedance measurement.

III. Modeled and experimental results

The multi-stage EMI modeling approach for high-frequency coupling to an I/O line was checked with measurements on a test board. The test board was a two-layer board with the entire solid bottom plane used as the reference. Two closely-spaced traces were routed on the top of the test board, as shown in Figure 3. The metallization on the top layer near the traces was removed and the remaining area was connected to the reference plane by copper tape and soldering at the edges of the board. The test board had a dimension of 12.5 $cm \times$ 5 cm, and the spacing between the top and bottom layers was 40 mils. The dielectric constant obtained from measurements was approximately 4.5. On the top plane, both of the traces were 13 $mils$ wide, 2 $oz.$ copper, and the edge-to-edge spacing was 16.5 $mils$ for a 3 cm coupled section. There were bonding pads at the ends of the traces for placing loads. The per-unit-length parameters of the coupled transmission lines were determined from measurements and numerical cross-sectional analysis [6]. The self and mutual inductances were 5.85 nH/cm and 2.16 nH/cm, and the self and mutual capacitances were 0.59 pF/cm and 0.2 pF/cm. Both traces had a characteristic impedance of approximately 100 Ω. For the I/O coupling study, a 20 cm wire with a diameter of 0.063 cm was soldered to the coupled I/O line at the board edge, and extended straight beyond the test board.

The input impedance of the EMI antenna was determined from the FDTD modeling and by measurements. The measurement configuration is shown in Figure 4. The bottom reference plane of the test board was used for placing an 0.085" semi-rigid coaxial cable in the center of the board, and the top plane of the test board was unused in this measurement. The shield of the semi-rigid cable was soldered to the ground plane along the length that traversed the board. At the edge of the board, the shield of the semi-rigid cable and the dielectric filling were removed, and the center conductor was used as the attached cable to replace the wire attached to the I/O line. The center conductor had a diameter of 0.063 cm, and extended 20 cm beyond the board edge. On the opposite side of the board, the semi-rigid cable was extended beyond the board edge by 2.5 cm, and then connected to an HP4291A impedance analyzer. An aluminum plate was introduced to separate the test fixture from the measurement equipment and cables, and avoid undesirable parasitic coupling. The plate was 62 $cm \times 62$ cm, and connected to the cable shield. The reference plane for the measurement was at the board edge where the center conductor was extended beyond the PCB edge.

The test configuration was also modeled with FDTD, and the input impedance determined. A sinusoidally modulated Gaussian pulse voltage source, with a source impedance of 50 Ω, was applied at the board edge to drive the extended center conductor against the test board reference plane. The aluminum plate as an extended ground structure was also included in the FDTD modeling. The conductors were modeled as perfect conductors (PECs), and a thin wire algorithm was applied for the center conductor [7]. The FDTD cell size was 0.6 $cm \times 1.25$ $cm \times 1.25$ cm. The time step was 1.6×10^{-11} s, and 3500 time steps were used for the calculation. Perfectly-matched-layer (PML) absorbing boundary conditions were also employed [8]. The voltage and the current at the source cell were recorded, and the input impedance of the EMI antenna was calculated from the Fast Fourier Transform (FFT) of the time history. In addition, the radiated field at 3 m away was calculated for evaluating EMI due to the coupled noise in later stages. The input impedance of the EMI antenna from the FDTD modeling and measurements agree well as shown in Figure 5. The center conductor and the test board reference plane were driven as a resonant quarter-wave dipole antenna at approximately 230 MHz, with an input impedance of 75 Ω. At the other resonant frequencies, such as 500 MHz, 1000 MHz, and 1304 MHz, the input impedance was on the order of 100 Ω.

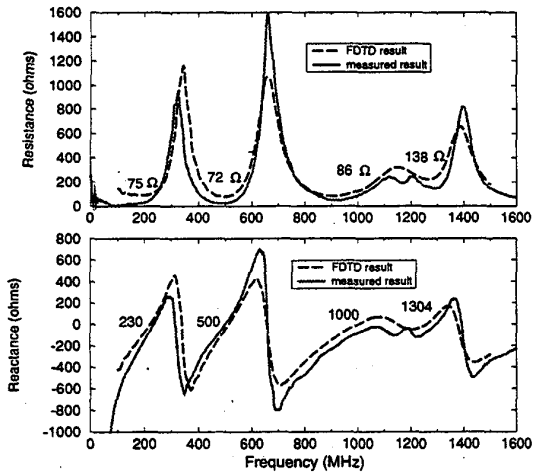

Figure 5. The input impedance of the EMI antenna for a cable attached to a PCB.

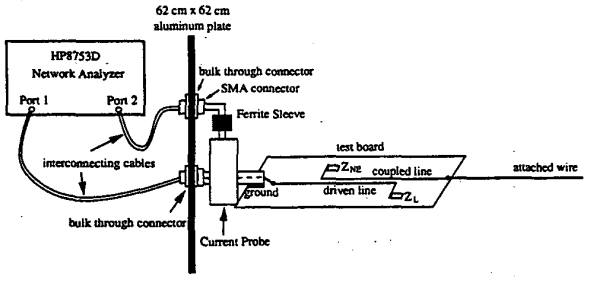

Figure 6. The configuration of the common-mode current measurements.

Common-mode current due to the high-frequency coupling to an I/O line was also measured through $|S_{21}|$. The test configuration is shown in Figure 6. An HP8753D network analyzer was used to measure the $|S_{21}|$. The two ports of the network analyzer were connected to the test fixture through the identical aluminum plate used in the input impedance measurements. Port 1 of the network analyzer was connected to the source line through an 0.085" semi-rigid coaxial cable. The shield of the cable was soldered to the ground of the top plane. A Fischer F-2000 current probe was clamped on the semi-rigid cable between the test board and the aluminum plate, and connected to Port 2 of the network analyzer. The ferrite sleeve on the connecting cable was used to minimize parasitic coupling. Z_L and Z_{NE} were the loads for the source circuit and the near-end of the coupled circuit, respectively. Two special cases were studied where Z_L and Z_{NE} were either open or short. The transfer function of the current probe was included in the network analyzer calibration procedure, and, as a result, the measured $|S_{21}|$ was related to the common-mode current I_{CM} due to the coupled noise as [9]

$$|S_{21}| = 50\ \Omega \times \left|\frac{I_{CM}}{V_s}\right|, \tag{2}$$

where V_s was the source voltage from Port 1 of the network analyzer.

The common-mode current on the cable at the plate was also calculated using the multi-stage modeling approach. The coupled section of the transmission lines were modeled with 32 lumped-element pi-sections. The remaining transmission line sections were modeled as ideal transmission lines, and the antenna input impedance was the load at the far-end of the I/O line. The circuit was then analyzed with SPICE, and the coupled noise voltage V_{noise}^{cl} at the location where the wire was attached was calculated. In the next step, the noise voltage was used to drive the wire against the reference plane of the test board, and the common-mode current on the semi-rigid cable at the aluminum plate was calculated to determine the $|S_{21}|$ from

$$|S_{21}| = 50\Omega \times \left|\frac{I_{CM}^{SMGP}}{V^{SMGP}}\right| \times \left|\frac{V_{noise}^{cl}}{V_s}\right|. \tag{3}$$

where the superscript $SMGP$ denotes the value calculated from the FDTD modeling with a sinusoidally modulated Gaussian pulse, V_{noise}^{cl} is the noise voltage determined from the coupled line problem, and V_s is the unit voltage excitation of the coupled line problem. For the two loading extremes chosen, the output impedance seen looking back into the coupled lines is not included, because it is small relative to the antenna impedance.

The measured and modeled results of $|S_{21}|$ are compared in Figure 7. In general, the results agree favorably up to 1.3 GHz. The peaks occurred at 230 MHz, 500 MHz, and 1100 MHz where the attached wire was driven resonant. Beyond 1.3 GHz, the calibration procedure was not adequate for the $|S_{21}|$ measurements. In addition, the artifacts associated with the connectors, the current probe, and the bonding pads were neglected in the modeling and contributed to the discrepancies between the measured and modeled results.

IV. EMI from Coupling to An I/O Line with Microstrip and Stripline Configurations

The multi-stage EMI modeling for coupling to an I/O line is useful for evaluating the EMI in microstrip and stripline geometries, and can be used to provide design direction for coupling length and line spacing. A few cases are provided herein for coupling and EMI in both the microstrip

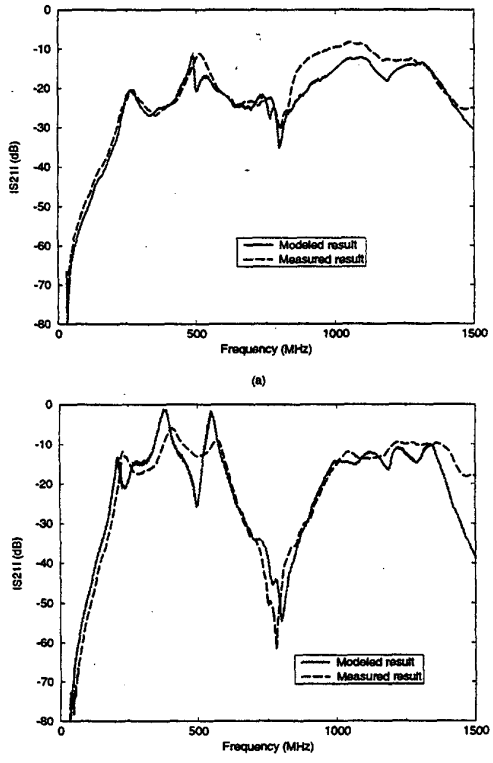

Figure 7. The modeled and measured results for $|S_{21}|$ (common-mode current) with (a) Z_L and Z_{NE} open, and (b) Z_L and Z_{NE} shorted.

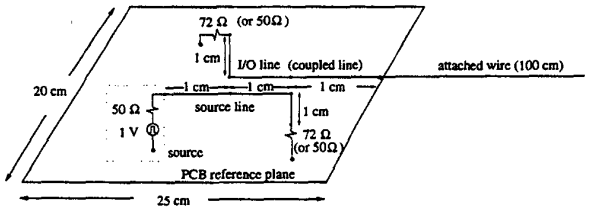

Figure 8. The configuration for the coupled transmission lines with an attached wire.

and stripline geometries. The modeled test board had a dimension of 25 cm × 25 cm, with an attached wire of 1 m long. The wire had a diameter of 40 $mils$ (AWG #18). The test board and the coupled transmission lines are shown in Figure 8. The coupled 1 cm section of the transmission lines had either a microstrip line structure or a stripline structure. The cross-section views of the structures are shown in Figure 9. The load of the source circuit and the near-end of the I/O circuit were both 72 Ω for the coupled microstrip lines, and 50 Ω for the coupled striplines, and matched the transmission lines. The inter-layer spacing was 10 $mils$, and the dielectric filling had a dielectric constant of 4.5. Both the microstrip and

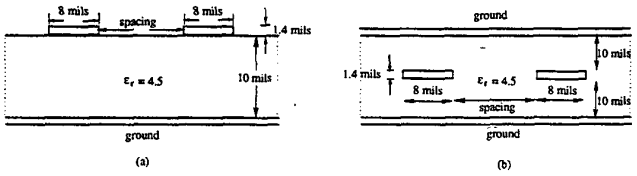

Figure 9. The cross-sectional view of (a) the coupled microstrip lines, and (b) the coupled striplines.

Table I. The per-unit-length parameters for coupled microstrip lines and striplines (L in nH/cm, C in pF/cm)

	Microstrip lines (1)	Microstrip lines (2)	Striplines (1)	Striplines (2)
L_{11}	4.199	4.280	3.367	3.431
L_{12}	1.099	0.057	0.473	0.141
C_{11}	0.824	0.792	1.517	1.462
C_{12}	0.128	0.00185	0.213	0.060
Z_o (Ω)	71.4	73.5	47.1	48.4

the stripline were 8 $mils$ wide, and 1 $oz.$ copper traces. Varying edge-to-edge spacing, from 1 line width to 10 line widths, was used in the EMI modeling to compare the radiated fields with the FCC Class B limit. As the first step of the multi-stage modeling, the per-unit-length parameters of the coupled transmission lines were extracted using numerical cross-sectional analysis tools. For example, the self parameters (L_{11} and C_{11}), mutual parameters (L_{12} and C_{12}), and characteristic impedance of the transmission lines (Z_o) are shown in Table I for coupled microstrip lines with (1) 1 line width spacing and (2) 10 line width spacing, and coupled striplines (1) with 1 line width spacing and (2) 2 line width spacing. A 1 V source with a 50 Ω impedance was used. The coupled transmission lines were modeled with 32 lumped-element pi-sections. Four cases of coupled lines, i.e., microstrip lines with 1 or 10 line width spacing, and striplines with 1 or 2 line width spacing, were modeled with SPICE to determine the noise voltage. Then the magnitude of the E-field at 3 m away was calculated from Eq.(1). The results are shown in Figure 10. The FCC Class B limit is also shown in these plots for comparison. For coupled lines with a microstrip structure, the radiated fields were significantly over the FCC limit for a line spacing less than 10 line widths (2 mm). For coupled lines with stripline structure, the coupling decreased rapidly with increasing line spacing. The radiated fields were under FCC limit for a spacing greater than 2 line widths.

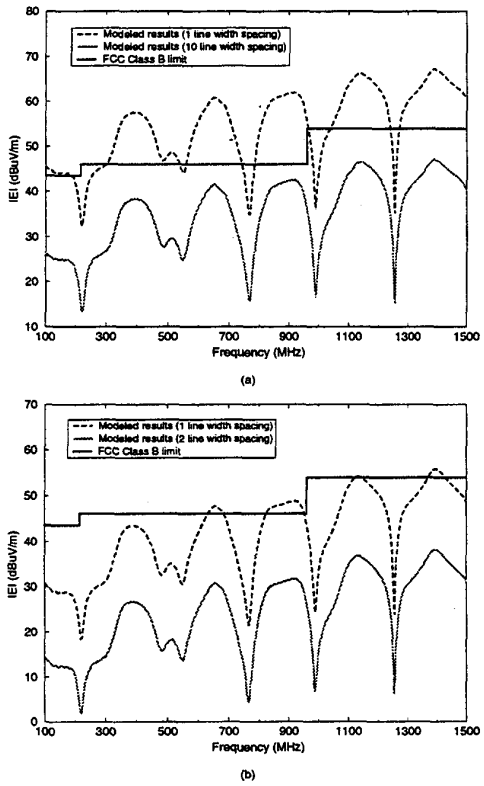

Figure 10. The radiated field for coupling between two (a) microstrip, and (b) striplines.

The 1 V source is particularly large for many cases. Further, the I/O line was unterminated, and unfiltered, and the cable unshielded. A terminated line with a single signal return reduces the EMI by approximately 6 dB [10]. However, these simple examples illustrate the utility of the multi-stage modeling approach. Further, they demonstrate that coupling and EMI can be significant even for coupled segments as short as 1 *cm*. Also, if the interconnect inductance of the shunt capacitors filtering the I/O line exceeds a few nanohenries, rendering the filtering ineffective in the hundreds of megahertz frequency range, the EMI consequences can be severe. Finally, the coupling and EMI for the stripline configuration is much less than the microstrip.

V. Conclusions

A multi-stage modeling approach was developed to anticipate the EMI resulting from coupling to I/O lines. Measurements on a test board showed favorable agreement with the modeling. Circuit analysis and FDTD modeling methods are used in the modeling stages to circumvent the complexity of full-wave modeling at the printed circuit level. Separating the radiation problem from the PCB coupling problem provides a faster way to estimate EMI from the PCB with good approximations. In addition, SPICE or IBIS device models, filtering, and line loss can be handled in the coupled transmission line study. From the estimate of the radiated fields, design guidelines can be developed for line spacing, microstrip and stripline structures, layer separations, rise time, and filtering.

References

[1] Y. Ji, M. W. Ali and T. H. Hubing, "EMC applications of the EMAP5 hybrid FEM/MOM code," *1998 IEEE International Symposium on Electromagnetic Compatibility*, Denver, Colorado, August 1998, pp. 543 - 546.

[2] C. R. Paul, *Analysis of Multiconductor Transmission Lines*, New York, NY: John Wiley & Sons, Inc., 1994.

[3] J. S. Roychowdhury and D. O. Perderson, "Efficient transient simulation of lossy interconnect," *28th ACM/IEEE Design Automation Conference*, pp. 740 - 745, 1991.

[4] C. R. Paul, *Introduction to Electromagnetic Compatibility*, New York, NY: John Wiley & Sons, Inc., 1992.

[5] T. Dhaene, and D. D. Zutter, "Selection of lumped element models for coupled lossy transmission lines," *IEEE Trans. on Computer-Aided Design*, vol. 11, no. 7, pp. 805 - 815, July 1992.

[6] W. Cui, H. Shi, X. Luo, J. L. Drewniak, T. P. Van Doren, and T. Anderson, "Lumped-element sections for modeling coupling between high-speed digital and I/O lines" *IEEE 1997 International Symposium on Electromagnetic Compatibility*, Austin, Texas, August 1997, pp. 260 - 265.

[7] A. Taflove, *Computational Electrodynamics: the finite-difference time-domain method*, Norwood, MA: Artech House, Inc., 1995.

[8] J. P. Berenger, "A perfectly matched layer for the absorption of electromagnetic waves," *Journal of Computational Physics*, vol. 114, no. 2, pp. 185 - 200, October 1994.

[9] D. M. Hockanson, J. L. Drewniak, T. H. Hubing, T. P. Van Doren, F. Sha, C. Lam and L. Rubin, "Quantifying EMI resulting from finite-impedance reference planes," *IEEE Trans. on Electromagnetic Compatibility*, vol. 39, no. 4, pp. 286 - 297, November 1997.

[10] X. Luo, M. Li, and J. L. Drewniak, "Time history extrapolation for FDTD modeling of shielding enclosure designs and EMI antenna geometries," *1998 IEEE International Symposium on Electromagnetic Compatibility*, Denver, Colorado, August 1998, pp. 1172 - 1177.